

## Cycle life performance of lithium-ion pouch cells

Karthikeyan Kumaresan, Qingzhi Guo, Premanand Ramadass, Ralph E. White\*

*Department of Chemical Engineering, University of South Carolina, Columbia, SC 29208, USA*

Received 26 June 2005; accepted 31 August 2005

Available online 15 November 2005

### Abstract

Cycle life studies have been done on lithium-ion pouch cell with  $\text{LiCoO}_2$  as cathode and meso-carbon micro-beads (MCMB) as anode at five different temperatures. By using the rate capability tests done at the same temperature as that of cycling and the half cell studies done on the fresh and cycled individual electrodes, the stoichiometric windows of individual electrodes at the beginning and at the end of cycling have been estimated. By analyzing these estimates along with the X-ray diffraction studies and half cell studies on cycled cathodes, scanning electron microscopy (SEM), energy dispersive spectroscopy (EDS) and half cell studies on cycled anodes, possible causes of increased capacity fade with increasing temperature were found to be the anode active material loss, probably due to a solvent/salt reduction reaction on the anode. Lithium deposition on the anode also has been identified as a possible side reaction during later stages of cycling at 35 and 45 °C.

© 2005 Elsevier B.V. All rights reserved.

*Keywords:* Capacity fade; Temperature dependence; Lithium-ion pouch cell; Stoichiometric windows

### 1. Introduction

Thermal and cycling stability and better Li-ion mobility of  $\text{LiCoO}_2$  make it the most preferred commercial cathode for Li-ion cells despite its high cost and relatively low capacity [1]. Similarly, meso-carbon micro-beads (MCMB) and other graphitized carbons are preferred as the anode material due to their low irreversible capacity and their low potential intercalation–deintercalation reactions [2]. Unfortunately, the capacity of Li-ion cells with these active materials fades as they are cycled and the rate of capacity fade depends on a number of cycling parameters like charge–discharge rate, end of charge voltage, end of discharge voltage, temperature, etc. [3,4].

In this work, the effect of temperature on the rate of capacity fade of lithium-ion ( $\text{LiCoO}_2/\text{MCMB}$  2528) pouch cells was studied experimentally. Rate capability tests were done at the same temperature as that of cycling in order to understand the conditions prevailing in the cell during cycling. By conducting the half cell studies on fresh and cycled individual electrodes the stoichiometric windows within which these electrodes operate at the beginning and at the end of cycling have been estimated. These estimates, when analyzed along with the X-ray diffraction

studies and half cell studies on cycled cathodes, scanning electron microscopy (SEM), energy dispersive spectroscopy (EDS) and half cell studies on cycled anodes and the rate capability studies on full cells give a better understanding of the capacity fade mechanisms.

### 2. Experimental

Lithium-ion pouch cells received from the National Reconnaissance Office were used for the cycling studies. The nameplate capacity of each cell is 1.66 Ah. Each cell consisted of four (two-sided) positive electrodes (cathodes) and five (three two-sided and two one-sided) negative electrodes (anodes). Some of the design parameters of individual electrodes are given in Table 1. The active materials of the positive and negative electrodes are stoichiometric lithium cobalt oxide ( $\text{LiCoO}_2$ ) and MCMB 2528, respectively. One molar  $\text{LiPF}_6$  in a quaternary solvent mixture of EC, PC, EMC and DEC was used as the electrolyte. Each of the four two-sided positive electrodes was bagged using the separator (Celgard). Each of the three two-sided negative electrodes was sandwiched between two positive electrode-containing separator bags while the two single-sided negative electrodes covered the outer positive electrodes. The entire assembly of anodes, cathodes and separators was enclosed by a proprietary material to make the pouch cell.

\* Corresponding author. Tel.: +1 803 777 3270; fax: +1 803 777 0793.  
E-mail address: [rew@sc.edu](mailto:rew@sc.edu) (R.E. White).

Table 1  
Design parameters of the Li-ion cell used in this study

Design parameter	Positive electrode	Negative electrode
Active material loading per side (g) (including binder and carbon)	2.211	1.020
Area of each side (cm <sup>2</sup> )	105.286	109.664
Electrode thickness (μm)	160	162

After the formation cycles (details of which are proprietary), the cells were cycled at five different temperatures, namely 5, 15, 25, 35 and 45 °C. Each cycle consisted of a constant current charging at  $C/2$  rate ( $C$  rate = 1.66 A) until the voltage reached an end of charge voltage of 4.1 V, a constant voltage charging at 4.1 V until the current tapered down to 50 mA and a constant current discharge at  $C/2$  rate until a cut-off voltage of 3.3 V. All cycling tests were done using Arbin BT-2000 battery testing systems. Tenny environmental chambers (Model T6S) were used for maintaining respective cycling temperatures and near zero humidity atmospheres.

Rate capability tests were done before cycling and at the end of every 100 cycles. The rate capability tests consisted of measuring the charge–discharge capacity of the cell at three different rates, namely  $C/33$ ,  $C/2$  and  $C$  in that order. For the  $C/33$  rate, the cell was first charged to 4.1 V and then discharged until the voltage reached 3.3 V. For  $C/2$  and  $C$  rates, cells were first charged up to 4.1 V at respective constant current rate followed by a constant voltage charging at 4.1 V until the current reached 50 mA. The subsequent discharge consisted of two stages. The first discharge was done at the respective rate ( $C/2$  or  $C$ ) until the voltage reached 3.3 V followed by a rest period of 30 min. The second stage discharge was done with a constant current of 50 mA (which is equal to the  $C/33$  rate).

The rate capability tests were done at the same temperature as that of cycling. This is in contrast with the method followed by other researchers: in most of the published capacity fade studies the periodic tests like rate capability, EIS, etc. were done at one particular temperature irrespective of the cycling temperatures with the intention of using those data to evaluate the effect of cycling temperature [6]. In other words, changes in the rate capability and impedance measured at chosen temperature were considered to be effects of cycling at various temperatures. In this work, by performing the rate capability tests at the same temperature as that of cycling, it was intended to analyze actual conditions prevailing inside a cell during cycling. The advantages of conducting these rate capability tests at respective cycling temperatures will be further elucidated in later sections of this paper.

At the end of cycling the cells were disassembled inside a glove box containing ultra pure argon for further studies. Before opening the cells they were discharged in two stages, first with 50 mA of current and the second with 20 mA of current with a rest period of 30 min between them, to ensure a complete discharge. Swagelok-type [7] half cells were made using the cycled electrodes (cut into round discs with a diameter of 7/16 in.) as working electrodes and lithium metal as the counter and refer-

ence electrode. The residual capacities of the electrodes were measured by discharging the electrodes, intercalation in case of cathodes and de-intercalation for anodes at a very small current (20 μA). Then the electrodes were charged using the same current to measure the intrinsic capacity of cycled electrodes. The surface of the negative electrodes was analyzed using a high vacuum scanning electron microscope. Energy dispersive analysis was used to analyze the elemental composition on the cycled anode surfaces. The crystallographic changes in the positive and negative active materials were analyzed using X-ray diffraction.

### 3. Results and discussion

#### 3.1. Initial performance analysis

##### 3.1.1. Initial charge–discharge performance

The variation of initial charge and discharge capacities measured at  $C/33$  rate is shown in Fig. 1. The initial charge capacity increases with increasing temperature. But the discharge capacity increases from 5 to 35 °C and then decreases. The columbic efficiency also decreases from 35 to 45 °C. One of the most important causes for the lower columbic efficiency is the possible repeated solid electrolyte interface (SEI) formation even after the formation cycles [3]. The fact that a lot of side reaction products were observed on the anodes of cells cycled at 35 and 45 °C, as explained in later sections, indicates the possibility of this side reaction. The increase in the charge capacity (for a given end of charge voltage and charge rate) with increasing temperature can be attributed to the temperature effect on the transport properties, such as solid and liquid phase diffusion coefficients and ionic conductivity. With increasing temperature, the diffusion coefficients in the liquid and solid phases and the conductivity of the liquid phase increase thus reducing the build-up of concentration gradient (during charge–discharge) in the solid and liquid phases [8]. As a result of this, for a given charge–discharge rate and end of charge–discharge voltage, the cells are charged (discharged) to higher extent with increasing temperature.

The following two sub-sections will explain in detail how, for a given cycling rate, end of charge voltage and end of discharge voltage, the individual electrodes of the cells are cycled between varying states of charge with increasing temperature.

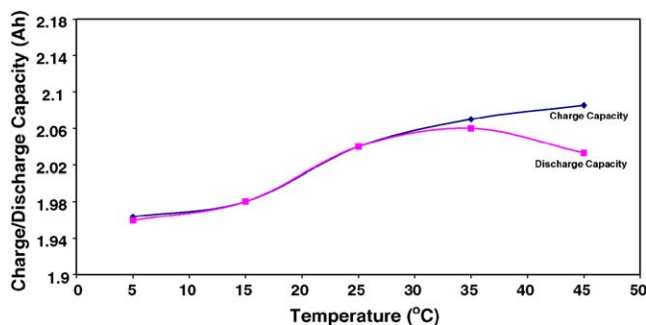


Fig. 1. Variation of initial charge–discharge capacity with increasing temperature.

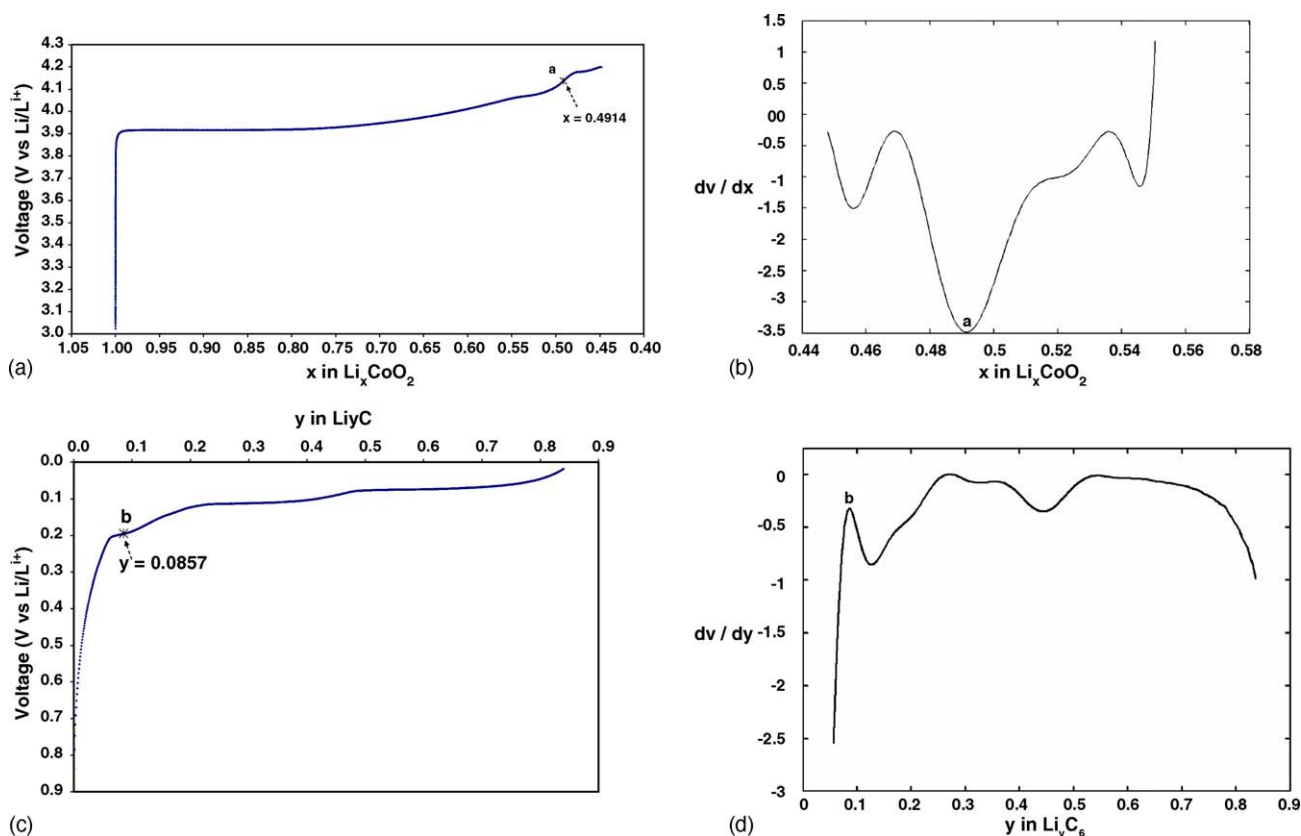


Fig. 2. (a) The potential (vs. Li/Li<sup>+</sup>) – state of charge profile of Li<sub>x</sub>CoO<sub>2</sub> half cell at C/33 rate. (b) First derivative of the potential vs. state of charge profile of Li<sub>x</sub>CoO<sub>2</sub>. (c) The potential (vs. Li/Li<sup>+</sup>) vs. state of charge profile of Li<sub>y</sub>C<sub>6</sub> half cell at C/33 rate. (d) First derivative of the potential vs. state of charge profile of Li<sub>y</sub>C<sub>6</sub>.

### 3.1.2. States of charge of individual electrodes

The anode and cathode active materials used to make a fresh lithium-ion cell are Li<sub>y</sub>C<sub>6</sub> and Li<sub>x</sub>CoO<sub>2</sub> (with  $y=0$  and  $x=1$ ), respectively. Based on the anode to cathode design capacity ratio and cyclable lithium loss due to SEI formation, the values of  $x$  and  $y$  at the beginning of cycling (at completely discharged state) will be different from that before the formation period [3,5]. The open circuit potential of Li<sub>x</sub>CoO<sub>2</sub> remains constant [9] for a broad range of  $x$  ( $x=0.74$ – $0.96$ ), whereas that of Li<sub>y</sub>C<sub>6</sub> remains constant ( $y=0.5$ – $1.0$ ). So, it is not possible to assume the state of charge of individual electrodes either at the beginning or at the end of charging of the full cell. By taking characteristic points of individual electrodes on a slow rate charge–discharge curve of a full cell as reference points, the state of charge of each individual electrode can be estimated with high accuracy. Fig. 2a shows the voltage – state of charge profile of Li<sub>x</sub>CoO<sub>2</sub> electrode with respect to Li/Li<sup>+</sup> electrode measured during a very slow rate (C/33 rate) charging. In order to identify a reference point on the slow rate charge profile of Li<sub>x</sub>CoO<sub>2</sub>, the derivative of the slow rate charge curve with respect to the state of charge of Li<sub>x</sub>CoO<sub>2</sub> ( $dV/dx$ ) has been plotted [10] as shown in Fig. 2b. During the charging (de-intercalation) of Li<sub>x</sub>CoO<sub>2</sub>, a rhombohedral to monoclinic phase transition occurs in the range  $x=0.5$ – $0.46$  [9]. Point ‘a’ ( $x=0.491$ ), where the  $dV/dx$  reaches a local minimum during de-intercalation, was chosen as a characteristic reference point as shown in Fig. 2a and b. Similarly, the voltage state of charge profile of Li<sub>y</sub>C<sub>6</sub> (Fig. 2c) has a charac-

teristic point at  $y=0.0857$  (point ‘b’), where the  $dV/dy$  (Fig. 2d) reaches a local maximum during intercalation. The initial slow rate (C/33 rate) charge profiles of full cells at different temperatures are shown in Fig. 3a and the differential plots ( $dV/dQ$ ) of the full cell charging profiles with respect to the charge capacity are shown in Fig. 3b. Since the charging rate is very slow, there is negligible concentration over-potential and the characteristics of individual electrodes are reflected on the full cell charge profile. Careful analysis of Fig. 3a and b along with Fig. 2a–d shows that the horizontal region A of Fig. 3a (corresponding to the local minimum A’ in Fig. 3b) is a characteristic of MCMB and the region B in Fig. 3a (corresponding to local maximum B’ in Fig. 3b) is a characteristic of Li<sub>x</sub>CoO<sub>2</sub>. Slow rate charging profile of full at 25 °C is shown in Fig. 3c. Points ‘a’ and ‘b’ in Fig. 2a and c, respectively, can be identified with points ‘a’ and ‘b’ in Fig. 3c. By knowing the state of charge of the anode at reference point ‘a’ and the state of charge of cathode at reference point ‘b’, the total loading of active material in the two electrodes and charge capacities before and after the reference points, the states of charge of individual electrodes at completely charged and at completely discharged state of the full cell can be estimated (Appendix A). Table 2 shows the estimates of the state of charge of each individual electrode at the beginning and end of full cell charging (at C/33 rate) at various temperatures. From Table 2 it is clear that with increasing temperature, the extent of charging of individual electrodes increases resulting in higher charge capacities.

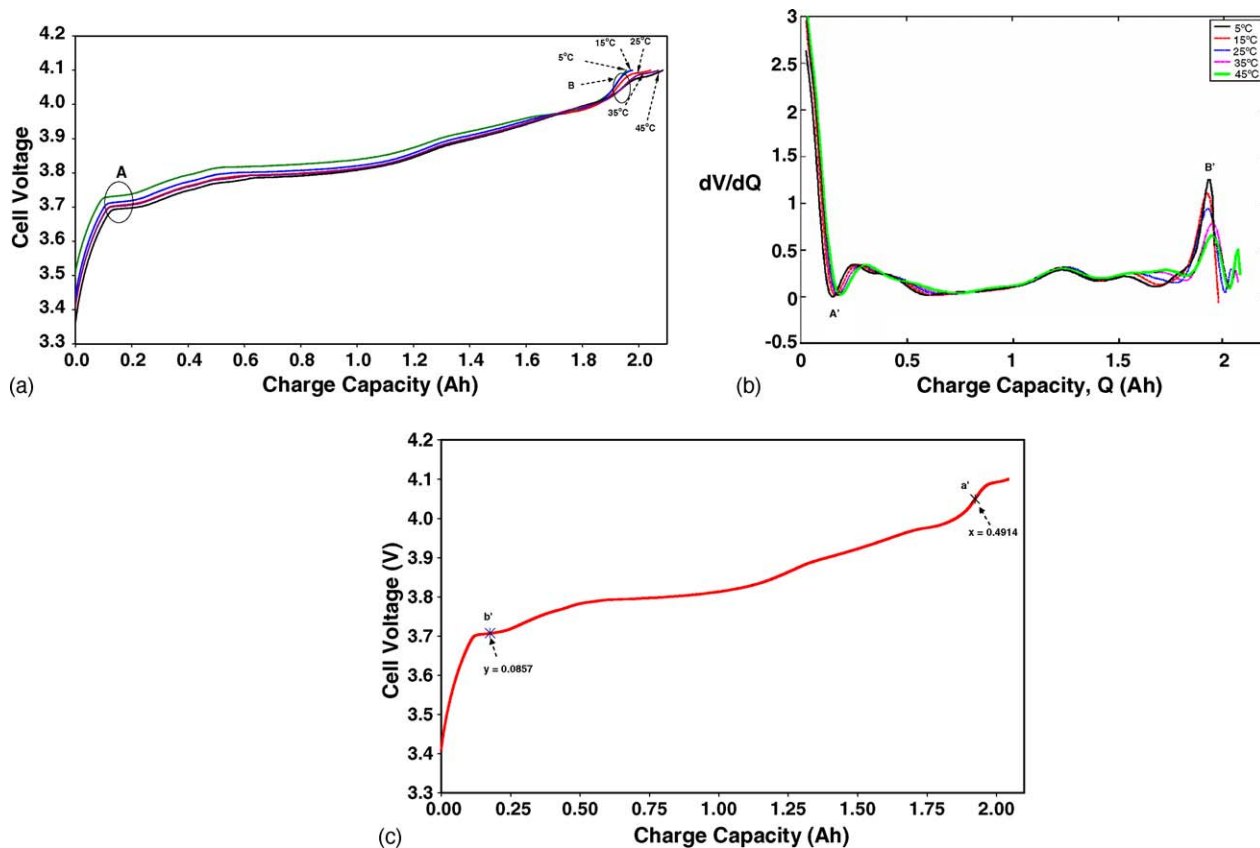


Fig. 3. (a) Slow rate (C/33) charge profiles of full cells at various temperatures. (b) First derivative of the cell voltage with respect to the charge capacity of full cell. (c) The slow rate (C/33) charging profile of full cell at 25 °C.

3.1.3. Initial rate capability

The rate capability measurements were done at the same temperatures at which the cells were cycled. The temperature dependence of discharge capacity at various rates is shown in Fig. 4. At all three rates, the discharge capacity decreases with decreasing temperature. Also at higher discharge rates, the discharge capacity decreases (with decreasing temperature) faster than at lower rates. This implies that for cycling tests, with fixed end of charge voltage and end of discharge voltage, at a given rate, the charge–discharge capacities at higher temperatures will be higher than at lower temperatures. So, the states of charge of individual electrodes at the beginning and at the end of a given cycle at a given charge–discharge rate will vary

with temperature. This can be further elucidated by analyzing the discharge profiles at different rates at a given temperature. Each of Fig. 5a–e presents the discharge profiles at three different rates (C/33, C/2 and C) for a given temperature. To obtain the above discharge profiles a rest period of 30 min at the end of C/2 or C rate (see vertical lines near the end of discharge in Fig. 5a–e) was used to eliminate the concentration polarization and the subsequent discharge at a very slow rate (C/33 rate) yielded the remaining available capacity. Depending on the temperature and the cycling rate, the state of charge (x in  $\text{Li}_x\text{CoO}_2$  and y in  $\text{Li}_y\text{C}_6$ ) of each individual electrode will vary at both the completely charged or completely discharged states of the full

Table 2

State of charge of individual electrodes (x in  $\text{Li}_x\text{CoO}_2$  and y in  $\text{Li}_y\text{C}_6$ ) at the completely charged and discharged state of the full cell at different temperatures

Temperature	$\text{Li}_x\text{CoO}_2$		$\text{Li}_y\text{C}_6$	
	Charged	Discharged	Charged	Discharged
5	0.4841	0.9344	0.7377	0.0314
15	0.4781	0.9322	0.7385	0.0263
25	0.4649	0.9323	0.7570	0.0224
35	0.4629	0.9377	0.7675	0.0229
45	0.4594	0.9377	0.7683	0.0182

The values in this table were estimated from the C/33 charge curve of the full cell.

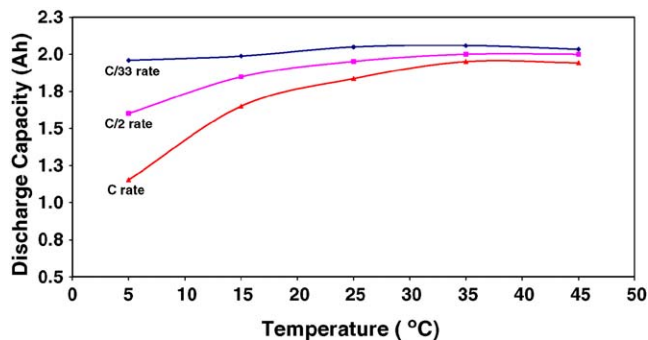


Fig. 4. Temperature dependence of discharge capacity at different discharge rates.

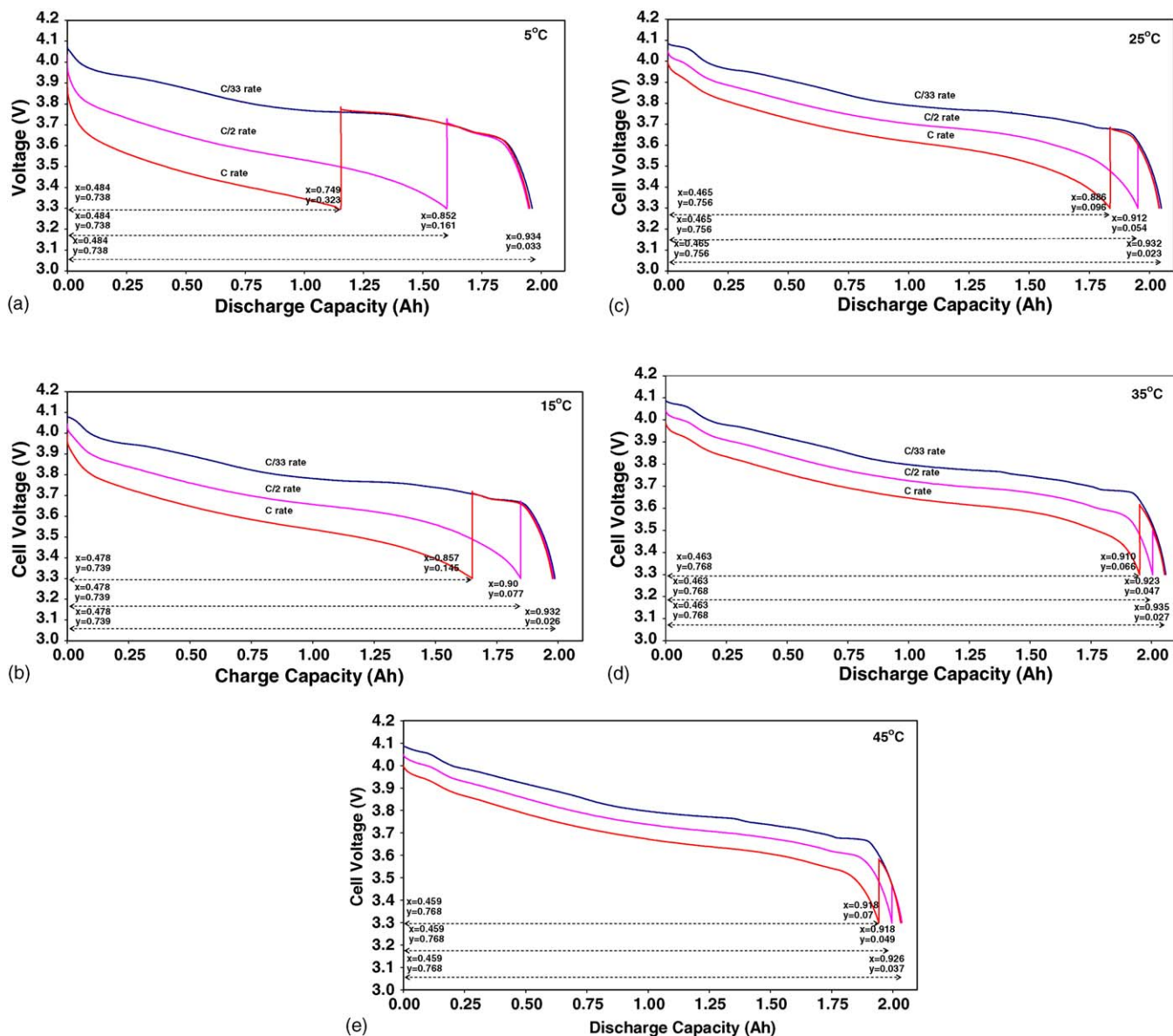


Fig. 5. Rate capability at various temperatures. The vertical lines of curves at the end of C/2 and C rates correspond to the 30 min relaxation period. The states of charge of anode (y in  $\text{Li}_y\text{C}_6$ ) and cathode (x in  $\text{Li}_x\text{CoO}_2$ ) are given at the beginning and end of discharge at each rate. (a) 5 °C, (b) 15 °C, (c) 25 °C, (d) 35 °C and (e) 45 °C.

cell (Fig. 5a–e). In other words, temperature and cycling rate determines the stoichiometric window within which the individual electrodes cycle.

### 3.2. Cycling performance

Cells at 5, 15 and 25 °C were cycled (as described earlier) 500 times, whereas the cells at 35 and 45 °C were cycled 200 times. The variation of discharge capacity with cycle number at various temperatures is shown in Fig. 6a. Though the initial discharge capacity increases with increasing temperature, the rate of capacity fade increases. Especially at temperatures higher than 25 °C (35 and 45 °C) the rate of capacity fade is drastically high. Fig. 6b shows the capacity fade calculated based on the total discharge capacity measured by two stages of dis-

charge, C/2 rate until the cell voltage reached 3.3 V and then C/33 rate until the cell voltage reached 3.3 V with a 30 min of rest in between, as a function of cycle number. The fraction of charge capacity obtained during the constant current charging period (% CC charge) decreases with cycling (Fig. 7) for all temperatures. During the first few cycles, the % CC charge increases with increasing temperature. But with cycling, the rate of decrease of the % CC charge increases drastically for higher cycling temperatures. This decrease in % CC charge might have been due to one or more of the following reasons: decrease in the transport properties of solid and liquid phases, and loss of active materials. All of the above three phenomena would have increased the concentration over-potential during charging which, in turn, would have caused the cell voltage to reach the cut-off (4.1 V) earlier.

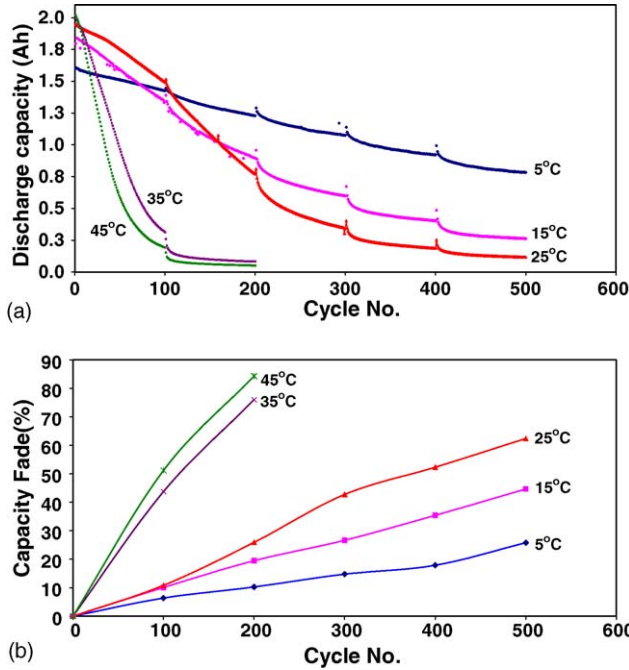


Fig. 6. (a) Variation of discharge capacity with cycling at C/2 rate. (b) Variation of capacity fades with cycling at various temperatures.

The variation of the slow discharge rate (C/33) performance with temperature at the end of 200 and 500 cycles are compared with that of the initial in Fig. 8a–c. The loss in slow rate performance with cycling increases with increasing temperature. Moreover, the drop in cell voltage during the slow rate discharge also increases with increasing temperature. The drop in voltage may be caused by a number of factors such as the increase in

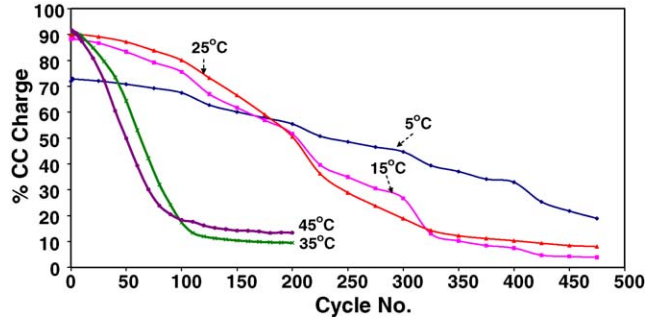


Fig. 7. Variation of percentage of charging done during constant current charging phase.

Ohmic resistance, loss of active material and resulting increase in impedance and concentration over-potential. The variation of Ohmic resistance ( $= \frac{\Delta V_{cell}}{I_{dis}}$ ) of the full cell estimated from the sudden voltage drop at the beginning of discharge is shown in the Fig. 9. At 5, 15 and 25 °C, the increase in the Ohmic resistance with cycling is gradual, whereas at 35 and 45 °C, it increases drastically.

### 3.3. Individual electrode analysis

At the end of cycling tests (500 cycles at 5, 15 and 25 °C and 200 cycles at 35 and 45 °C) the cells were disassembled for the individual electrode analysis. Prior to disassembly, all the cells were discharged at very low rate (20 mA) in order to make sure that all the cells were opened at completely discharge state. X-ray diffraction studies and half cell studies were performed on the cathode while scanning electron microscopy,

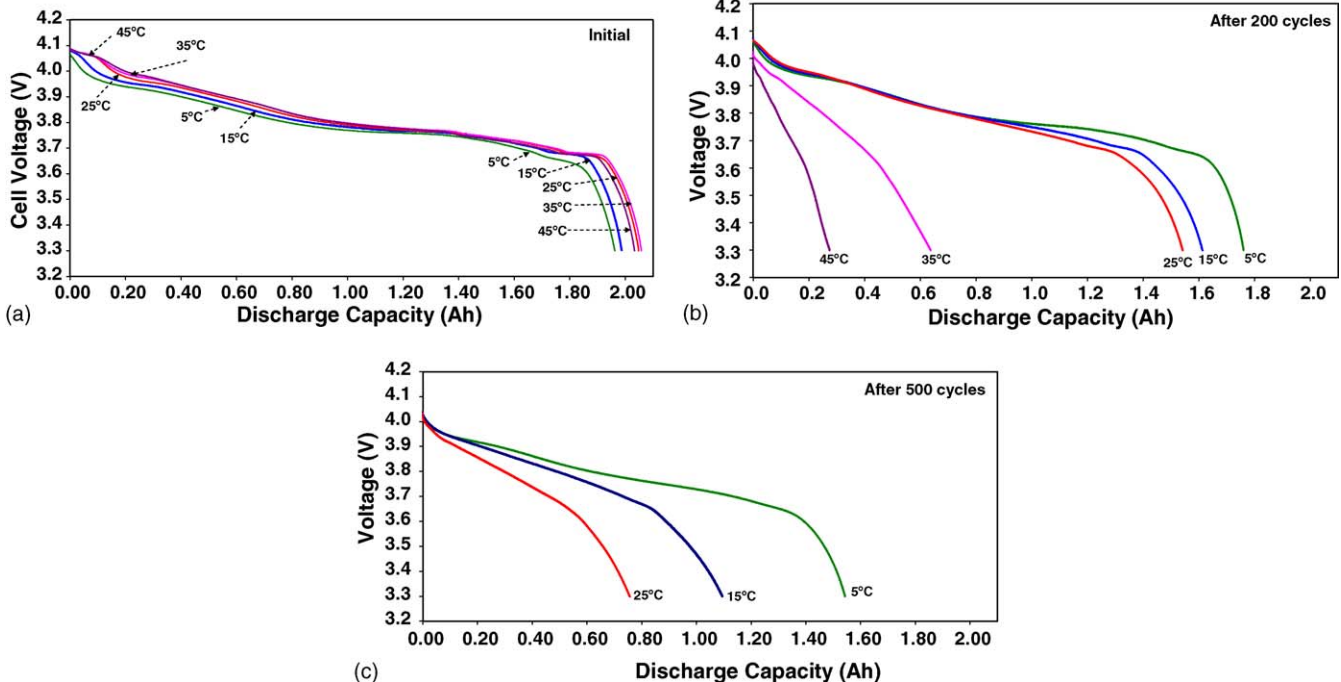


Fig. 8. (a) Comparison of slow rate (C/33) discharge profiles before cycling. (b) Comparison of slow rate discharge profiles at the end of 200 cycles. (c) Comparison of slow rate discharge profiles at the end of 500 cycles.

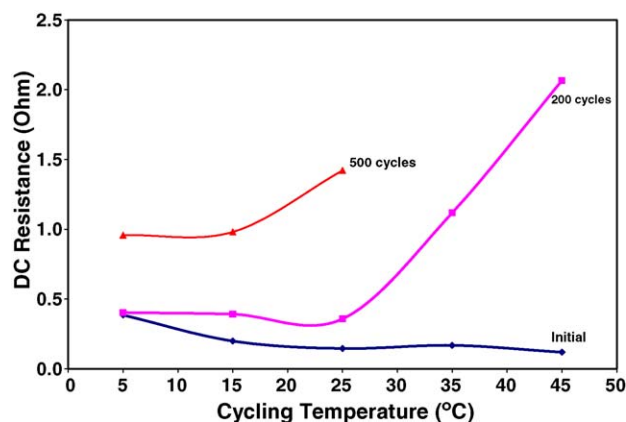


Fig. 9. Variation of Ohmic resistance of full cell with cycling at different temperatures.

energy dispersive analyses and half cell studies were done on anode.

### 3.3.1. Cathode analysis

The X-ray diffraction patterns of the cathode materials from the cells cycled at different temperatures are compared with that of the pure  $\text{LiCoO}_2$  in Fig. 10. A general observation is that there is no significant change in the XRD pattern, but there are some minor shifts in the (003) peaks towards lower diffraction angles indicating that the lattice parameter  $c$  increases with increasing cycling temperature. It has been reported in the literature that the lattice parameter  $c$  is a function of  $x$  in  $\text{Li}_x\text{CoO}_2$  [11]. It increases from 14.05 Å for  $x=1$  to a maximum of 14.41 Å at  $x=0.45$ , and then decreases reaching a minimum at  $x=0$ . The values of  $c$  for the electrodes cycled at different temperatures are given in Table 3. With increasing temperature, the value of  $c$  increases indicating that the cathodes were not completely discharged even though the full cells were discharged at a very low rate of 20 mA before they were disassembled. Half cell studies confirmed that the cathodes were not completely discharged. The half cells were first discharged at a very low rate (20  $\mu\text{A}$ ) to

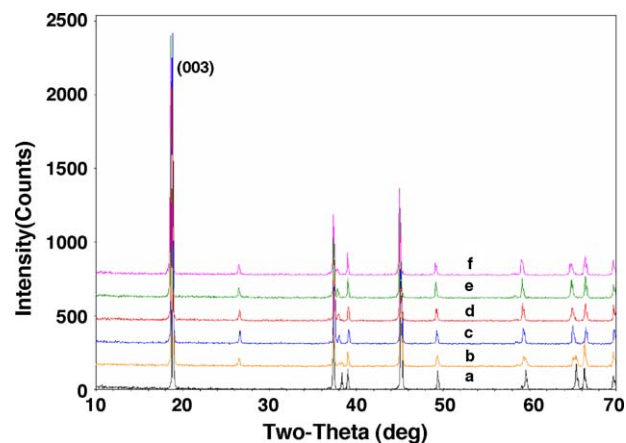


Fig. 10. XRD pattern of cathode materials: (a) fresh, (b) after 500 cycles at 5 °C, (c) after 500 cycles at 15 °C, (d) after 500 cycles at 25 °C, (e) after 200 cycles at 35 °C and (f) after 200 cycles at 45 °C.

Table 3

Relation between the lattice parameter  $c$  (calculated using the XRD studies) and the residual capacity of cathode cycled (estimated using half cell studies on cycled cathodes with 7/16 in. diameter) at various temperatures

Cycling temperature (°C)	$c$ Parameter (Å)	Residual capacity (mAh)	Actual capacity (mAh)
5	14.127	0.48	2.72
25	14.170	0.61	2.62
45	14.250	1.40	2.58

The actual capacity obtained during the subsequent charging of half cell is also given.

measure the residual capacity of the cathode (Table 3). The residual capacities thus measured increases with increasing cycling temperature. The initial discharge was followed by constant current charging at 200  $\mu\text{A}$  (which corresponds to  $C/15$  rate) until the potential of cathode reaches 4.3 V versus  $\text{Li}/\text{Li}^+$  and then charged at a constant voltage of 4.3 V until the charging current tapered down to 20  $\mu\text{A}$ . Under above charging conditions and electrode dimensions (7/16 in. in diameter), the charge capacity of the fresh cathode was 2.79 mAh. Fig. 11 compares the charging profiles of cathodes cycled at various temperatures with that of fresh cathode. The charge capacities of all the cathodes (Table 3), irrespective of the cycling temperature, did not vary much from the charge capacity of a fresh cathode. For the cycled electrodes, a considerable part of charging is done under the constant voltage phase since the cut-off voltage is reached quicker than that for the fresh cathode. This indicates that the impedance of the cathode has increased with cycling. If the cycled cathodes were to be charged at an even lower rate then their charge capacities would be equal to that of the fresh cathode.

### 3.3.2. Anode analysis

Random samples of anodes obtained from full cells cycled at various temperatures were observed under a scanning electron microscope. The anode surfaces of samples cycled at 5 and 15 °C did not have any apparent morphological change when compared to that of fresh anode (Fig. 12a). The surfaces of inner anodes from the cells cycled at 25 °C were covered by few patches of reaction products. All the anodes obtained from the full cells cycled at 35 and 45 °C were covered by a sig-

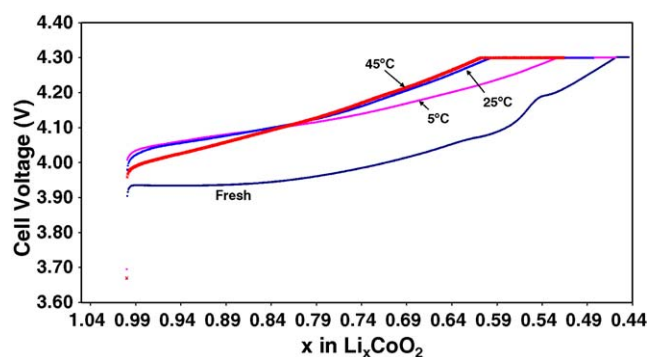


Fig. 11. Comparison of low rate ( $C/15$ ) charging profiles of fresh and cycled  $\text{Li}_x\text{CoO}_2$  electrodes.

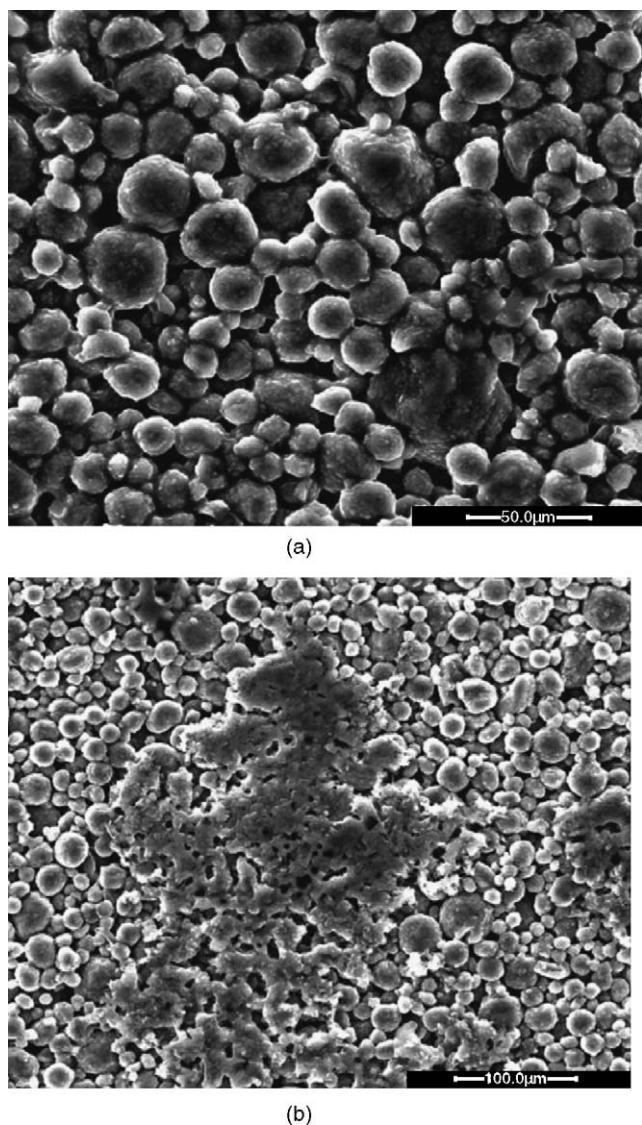


Fig. 12. (a) Scanning electron micrograph of a typical anode cycled at 15 °C. (b) Scanning electron micrograph of a typical anode cycled at 45 °C.

nificant amount of similar reaction products. Fig. 12b shows a typical patch found on the surface of the anode cycled at 45 °C. Energy dispersive analysis showed a distinct difference between the surface compositions on a clear area of the anode and on the patch of reaction products (Table 4). The patch contains 2.2%

Table 4  
Comparison of elemental composition on a cycled anode with clear surface and on a cycled anode with a patch of reaction product

Element	Weight %	
	On a clear area	On the patch
Carbon	85.49	69.10
Oxygen	7.48	20.53
Fluorine	5.96	8.18
Phosphorus	0.35	1.54
Copper	0.72	0.65
Total	100.00	100.00

more fluorine, 1.2% more phosphorus and 13.0% more oxygen compared to clear areas of the anode indicating that these patches are products of side reactions involving the electrolyte (possibly reactions forming  $\text{Li}_2\text{CO}_3$ ,  $\text{LiF}$ , etc.). The available active material in the anodes cycled at various temperatures was determined using the half cell studies. First the half cells were discharged (de-intercalation) using a very low current (20  $\mu\text{A}$ ) until the voltage reached 2.0 V. This was followed by a low rate (20  $\mu\text{A}$ ) charge (intercalation) until the voltage reached 10 mV. From the intercalation capacities thus obtained the amount of active material available on the cycled anode was calculated. It was found that 7.64  $\text{mg cm}^{-2}$  (the area here is the apparent geometrical area of the anode) of active material (MCMB) was available on the anode cycled at both 5 and 25 °C, whereas only 1.53  $\text{mg cm}^{-2}$  were available on the anode cycled at 45 °C. The fresh anode had an active material loading of 8.51  $\text{mg cm}^{-2}$ . From these calculations it is clear that the anode active material has been lost with cycling at all temperatures with the loss being severe above 25 °C. Since most of the anode in the cells cycled at 35 and 45 °C were covered by reaction products, making them less accessible or unavailable for the intercalation reaction, rate capability of the full cell may also decrease. Thus, the drastic decrease in the slow rate discharge performance (Fig. 8a–c) can be considered to be due to the isolation of anode active material (by the products of side reactions at the anode surface), the loss of cyclable lithium during the side reactions and the resulting decrease in the rate capability.

#### 3.4. Stoichiometric window and the capacity fade

Some interesting conclusions evolve when the cycling performance data (Section 3.3) are analyzed in the light of the initial rate capability and the stoichiometric windows at the beginning and at the end of cycling. From the half cell studies and XRD analysis of cathodes of cycled cells it is clear that there is no loss of cathode active material at any of the five temperatures. Depending on the initial anode–cathode capacity ratio, cycling conditions like temperature, charge–discharge rate, end of charge voltage and end of discharge voltage the stoichiometric windows of the individual electrodes can be expected to vary with cycling. The stoichiometric windows at the beginning of the cycling can be estimated by using the characteristic points of individual electrodes appearing on the slow rate discharge curve of full cells as reference points as shown in previous sections. Since the residual capacities available in the cycled electrodes have been estimated by half cell studies as described in Section 3.3, the completely discharged states ( $x = 1$  in  $\text{Li}_x\text{CoO}_2$  and  $y = 0$  in  $\text{Li}_y\text{C}_6$ ) can be taken as the reference points and the stoichiometric windows of individual electrodes during the last cycle (500th cycle for 5–25 °C and 200th cycle for 35 and 45 °C) can be back calculated. Table 5a and b show the stoichiometric windows of individual electrodes at the beginning and end of cycling at three different temperatures (5, 15 and 25 °C). At the beginning of cycling the cathodes are charged to higher degrees with increasing temperature ( $x$  in  $\text{Li}_x\text{CoO}_2$  at the end of charging is 0.484 for 5 °C and 0.459 for 45 °C). But during the last cycle the cathodes are charged to a lower degree ( $x$  in  $\text{Li}_x\text{CoO}_2$  at the end

Table 5  
Stoichiometric windows of individual electrodes

Cycling temperature (°C)	Cycle number	$x$ in $\text{Li}_x\text{CoO}_2$		$y$ in $\text{Li}_y\text{C}_6$	
		Charged	Discharged	Charged	Discharged
(a) Before cycling					
5	Initial	0.484	0.852	0.738	0.161
25	Initial	0.465	0.912	0.756	0.054
45	Initial	0.459	0.918	0.768	0.049
(b) After cycling					
5	500	0.54	0.73	0.7	0.36
25	500	0.52	0.563	0.4	0.48
45	200	0.58	0.611	1.13	1.01

These stoichiometric windows are calculated for  $C/2$  charge–discharge rates.

of charging is 0.54 at 5 °C and 0.58 at 45 °C). Even though the cathodes are charged to a higher state (smaller  $x$  in  $\text{Li}_x\text{CoO}_2$ ) during initial cycles, the state of charge of cathodes at the end of charging decreases with cycling. This is consistent with the observations that there are no significant losses of cathode active material (half cell studies) and that there is no cobalt dissolution (from energy dispersive analysis on the anode) due to cycling.

A significant amount of reaction products (most probably from reactions involving the electrolyte) were found on the anode surface of cells cycled at high temperatures (35 and 45 °C). Some of the most possible side reaction at the anode is lithium deposition, solvent and salt reduction with film formation (even after the formation cycles). At the beginning of cycling, the maximum lithium content in the anode ( $y$  in  $\text{Li}_y\text{C}_6$ ) at the end of charging was only 0.768 (at 45 °C). Moreover, the rate capability of the cells during the initial cycles increases with increasing temperature indicating better solid and liquid transport properties. Solvent or salt reduction may be the main side reaction during the initial cycles since lithium metal deposition is not probable [12] under the aforementioned conditions. The products of these (solvent/salt reduction) reactions may increase the thickness of SEI layer, which will decrease the rate capability of anode. If the rate of side reaction is sufficiently high the reaction product may cover a significant part of the anode surface as seen on the anodes cycled at 35 and 45 °C. The anode active materials (MCMB) in the areas that are covered by the reaction products will no longer be available for intercalation–de-intercalation reactions. This decrease in the available active material will also decrease the rate capability of the full cell. This is reflected in the decrease in the width of stoichiometric window of the anode with cycling (Table 5a and b). The anode active material loss (due to the surface coverage by reaction products) above 25 °C is so high (only 17% of anode active material is available after 200 cycles at 45 °C) that the full cell becomes anode limited with cycling. As a result of this the anode is over-charged ( $y$  in  $\text{Li}_y\text{C}_6$  is 1.13 during the 200th cycle at 45 °C). The rate of side reactions and the resulting active material loss on the anodes of cells cycled at 35 and 45 °C is so high that during the course of the cycling tests the anodes began to get over-charged which probably resulted in lithium metal deposition [12], and hence capacity fade increases further.

#### 4. Conclusions

Cycling tests have been performed on Li-ion pouch cells containing  $\text{Li}_x\text{CoO}_2$  as the cathode and MCMB as the anode at five different temperatures (5, 15, 25, 35 and 45 °C). Using rate capability tests ( $C/33$ ,  $C/2$  and  $C$  rate) and half cell tests on the fresh (after formation) and cycled individual electrodes, the stoichiometric windows of individual electrodes were estimated at the beginning and at the end of cycling. X-ray analysis and half cell studies on the cathode material indicate that there is no significant loss of cathode active material. The fact that the extent of charging of the cathodes, at all the cycling temperatures, decrease ( $x$  in  $\text{Li}_x\text{CoO}_2$  at the end of charging decreases) with cycling verifies this result. The only significant change on the cathode with cycling is the increase in its impedance, which was reflected in the fact that the most of the charging of the half cells (made of cycled electrodes) was done in the constant voltage mode. The available active anode material decreases with cycling at all temperatures with the rate of decrease being drastic above 25 °C. Solvent or salt reduction were suggested as the most probable side reactions at the anode during the initial cycles at all temperatures. At 35 and 45 °C anode over-charging, and hence lithium metal deposition was also found to be a possible side reaction during the later part of the cycling.

#### Acknowledgement

The authors would like to acknowledge the financial support by the National Reconnaissance Office (NRO) under the contract # NRO-000-03-C-0122 in pursuing this project.

#### Appendix A

The procedure for estimating stoichiometric windows of individual electrodes using the  $C/33$  rate charge profile of individual electrodes and similar low rate charging profile of full cell:

For the  $\text{Li}_x\text{CoO}_2$  electrode at room temperature (25 °C):

By comparing with the point ‘a’ in Fig. 2a, the value of  $x$  in  $\text{Li}_x\text{CoO}_2$  at the point ‘a’ in Fig. 3c is = 0.4914.

Based on the total mass of cathode active material and the specific capacity of  $\text{LiCoO}_2$  ( $274 \text{ mAh g}^{-1}$ ), the theoretical capacity of the cathode is  $= 4.36 \text{ Ah}$ .

Charge capacity at  $C/33$  rate and  $25^\circ\text{C}$  is  $= 2.0422 \text{ Ah}$ .

Charge capacity at  $C/33$  rate and  $25^\circ\text{C}$  until the point 'a'  $= 1.9226 \text{ Ah}$ .

Therefore, the value of  $x$  in  $\text{Li}_x\text{CoO}_2$  at the beginning of the charging is given by

$$x = 0.4914 + \frac{1.9226}{4.36} = 0.9323$$

The value of  $x$  in  $\text{Li}_x\text{CoO}_2$  at the end of charging is given by

$$x = 0.4914 - \frac{(2.0422 - 1.9226)}{4.36} = 0.4649$$

For the  $\text{Li}_y\text{C}_6$  electrode at room temperature ( $25^\circ\text{C}$ ):

By comparing with the point 'b' in Fig. 2c, the value of  $y$  in  $\text{Li}_y\text{C}_6$  at the point 'b' in Fig. 3c is  $= 0.0857$ .

Based on the total mass of anode active material and the specific capacity of  $\text{Li}_y\text{C}_6$  ( $372 \text{ mAh g}^{-1}$ ), the theoretical capacity of the anode is  $= 2.78 \text{ Ah}$ .

The charge capacity of the full cell at  $C/33$  rate and  $25^\circ\text{C}$  until the point 'b'  $= 0.1758 \text{ Ah}$ .

Therefore, the value of  $y$  in  $\text{Li}_y\text{C}_6$  at the beginning of the charging of the full cell is given by

$$y = 0.0857 - \frac{0.1758}{2.78} = 0.0224$$

The value of  $y$  in  $\text{Li}_y\text{C}_6$  at the end of charging of the full cell at  $C/33$  rate is given by

$$y = 0.0857 + \frac{(2.0422 - 0.1758)}{2.78} = 0.7570$$

Similar calculations were done for the full cell charging at all other temperatures to obtain the values shown in Table 2.

## References

- [1] W.A. van Schalkwijk, B. Scrosati, *Advances in Lithium-ion Batteries*, Kluwer Academic/Plenum Publishers, New York, 2002.
- [2] M. Egashira, S. Okada, J. Yamaki, *J. Power Sources* 124 (2003) 237–240.
- [3] P. Arora, R.E. White, *J. Electrochem. Soc.* 145 (10) (1998) 3627.
- [4] P. Ramadass, B. Haran, R.E. White, B.N. Popov, *J. Power Sources* 111 (2002) 210–220.
- [5] J. Christensen, J. Newman, *J. Electrochem. Soc.* 152 (4) (2005) A818.
- [6] PNGV Test Plan for Advanced Technology Development Gen 2 Lithium-ion Cells, EHV-TP-121, Rev 6, October 5, 2001.
- [7] Q. Guo, R.E. White, *J. Electrochem. Soc.* 152 (2) (2005) A343.
- [8] L.O. Valoen, J.N. Reimers, *J. Electrochem. Soc.* 152 (5) (2005) A882.
- [9] Y. Shao-Horn, S. Levasseur, F. Weill, C. Delmas, *J. Electrochem. Soc.* 150 (3) (2003) A366.
- [10] I. Bloom, A.N. Jansen, D.P. Abraham, J. Knuth, S.A. Jones, V.S. Battaglia, G.L. Henriksen, *J. Power Sources* 139 (2005) 295–303.
- [11] G.G. Amatucci, J.M. Tarascon, L.C. Klein, *Solid State Ionics* 83 (1996) 167–173.
- [12] P. Arora, M. Doyle, R.E. White, *J. Electrochem. Soc.* 146 (10) (1999) 3543.